

Chapter 1

Results of Scientific Research on the completed Space Projects, obtained by Russian Scientists in 2016 – 2017

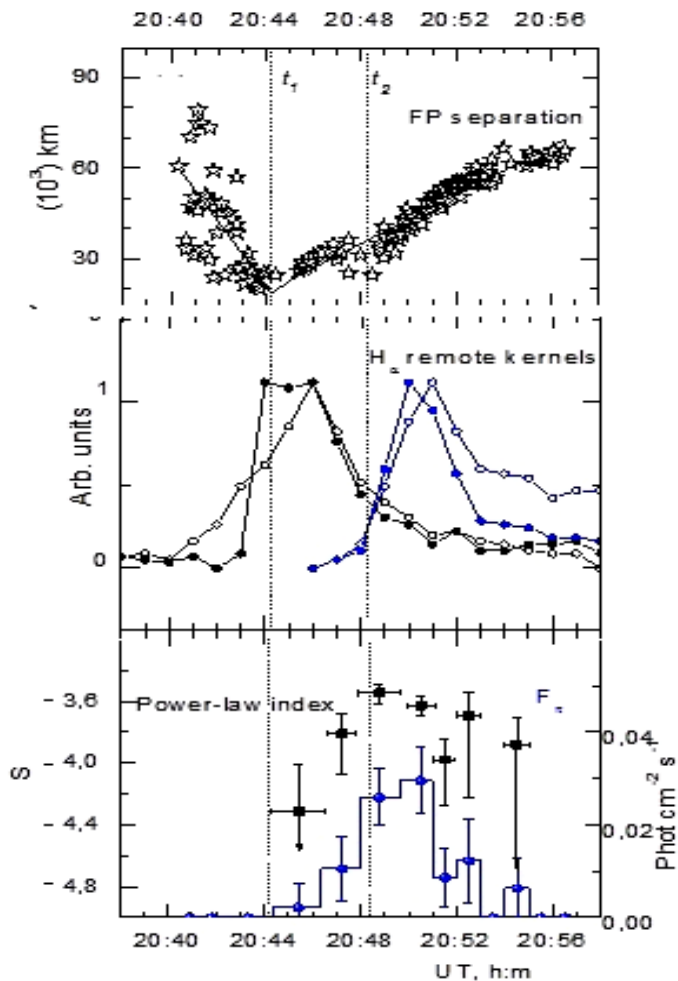
CONTENT

- 1.** Skobeltsyn Institute of Nuclear Physics of Lomonosov Moscow State University
- 2.** Russian Academy of Sciences, Space Research Institute
- 3.** Russian Academy of Sciences, Pushkov Institute of Terrestrial Magnetism, Ionosphere and Radio Wave Propagation
- 4.** Russian Academy of Sciences, Lebedev Physical Institute
- 5.** Russian Academy of Sciences, Kol'skiy Scientific Center, Polar Geophysical Institute
- 6.** Russian Academy of Sciences, Institute of Applied Physics
- 7.** Russian Academy of Sciences, Pulkovo Observatory
- 8.** National Research Nuclear University “MEPhI”

1.1. Study of proton acceleration in solar flares using gamma-ray observations

(Skobeltsyn Institute of Nuclear Physics of Lomonosov Moscow State University)

Appreciable hard X-ray (HXR) and gamma-rays emissions in the 0.04–150 MeV energy range associated with the October 29, 2003 solar flare (X10/3B) were observed at 20:38–20:58 UT by the SONG instrument onboard the CORONAS-F mission. To restore flare gamma-rays spectra we fitted the SONG energy loss spectra with a three-component model of the incident spectrum: (1) a power law in energy, assumed to be due to electron bremsstrahlung; (2) a broad continuum produced by prompt nuclear de-excitation gamma-lines; and (3) a broad gamma-line generated from pion-decay. We also restored spectra from the RHESSI data, compared them with the SONG spectra and found a reasonable agreement of these spectra in the 0.1–10 MeV energy range. The pion-decay emission was observed from 20:44:20 UT and had its maximum at 20:48–20:51 UT. The power-law spectral index of accelerated protons estimated from the ratio between intensities of different components of gamma rays changed with time. The hardest spectrum with a power-law index $S = -3.5 - 3.6$ was observed at 20:48–20:51 UT. Time



histories of the pion-decay emission and proton spectrum were compared with changes of the locations of flare energy release as shown by RHESSI hard X-ray images and remote H_αbrightenings. An apparent temporal correlation between processes of particle acceleration and restructuring of flare magnetic field was found. In particular, the protons were accelerated to subrelativistic energies after radical change of the character of footpoint motion from a converging motion to a separation motion.

Fig. 34. Upper panel: the distance between conjugated footpoints. Middle panel: intensities of the major remote H_α brightening patches in the eastern (black curves) and southern (blue curves) sites. Filled and unfilled circles correspond to different kernels. Bottom panel: flux of the pion-decay emission (blue points) and proton power-law spectrum index.

Selected publication

Kurt V.G., Yushkov B. Yu., Galkin V. I., Kudela K., Kashapova L.K. CORONAS-F observation of gamma-ray emission from the solar flare on 2003 October 29. *New Astronomy*, V.56, P.102-112. [Doi.org/10.1016/j.newast.2017.05.002](https://doi.org/10.1016/j.newast.2017.05.002)

1.2. Dynamics of relativistic electrons of the outer radiation belt

(Skobeltsyn Institute of Nuclear Physics of Lomonosov Moscow State University)

An abrupt decreases – dropouts in the population of energetic electrons in the Earth's outer radiation belt during magnetic storms are mentioned in many publications by a loss of electrons at $L=4-7$ resulting from their precipitation into the atmosphere or escape through the magnetopause. In the present study, the dropouts of electrons are explained primarily by adiabatic transformation of the magnetic drift trajectories. This conclusion was based on the analysis of dawn-dusk asymmetry of the electron latitudinal profiles measured by low altitude polar orbiters SERVIS-1 and

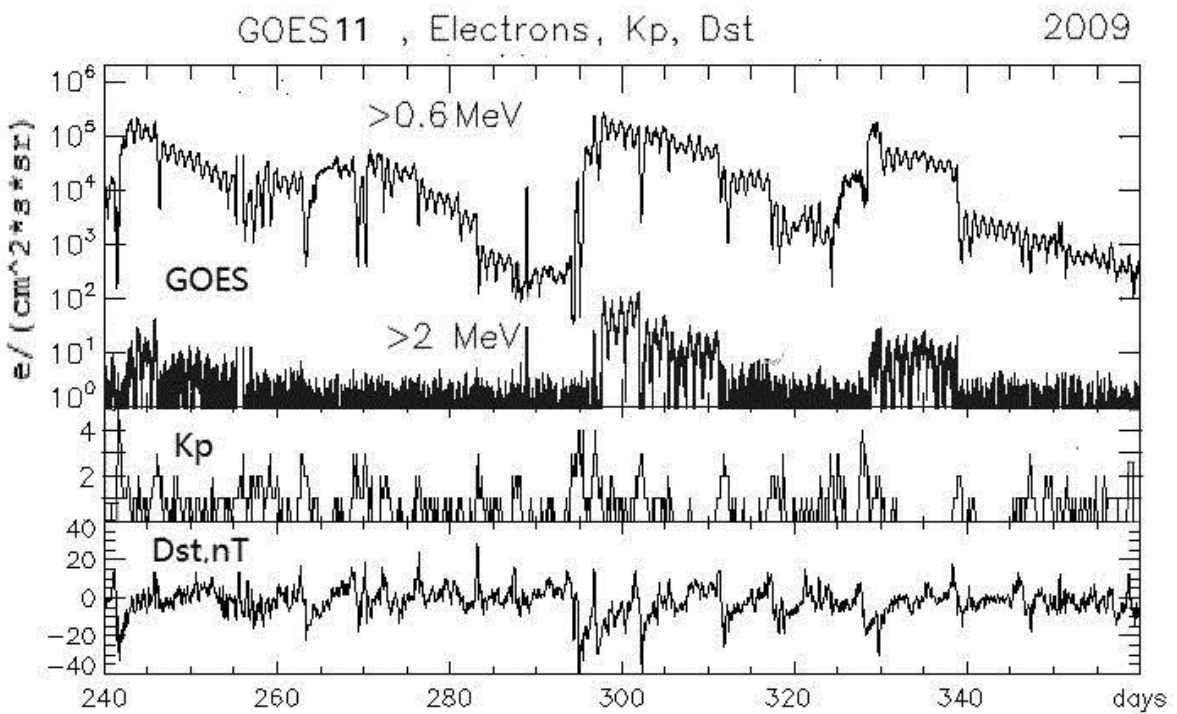
CORONAS-F and on the coincidence of pre-storm and after-storm profiles of radiation belt electrons and protons.

During the years of high and moderate activity increases of the energetic flux of electrons at geostationary region are compensated by the losses and as a result the overall level of the population persists. The transitions from high to low intensity and back by 3-4 orders of magnitude are fast within hours and caused by the magnetic disturbances, storms and substorms.

During the years of the low activity, the balance of increases and losses is violated, the whole flux of electrons is reduced. Particularly noticeable was the devastation of the outer belt during the minimum of 2009-2010 years. The slow type of decreases became most active as shown by Fig.38. The transition from the fast

type to the slow type of decreases was created by the prolonged periods of the low substorm activity. The slow type of intensity decreases is mostly probably caused by the losses on the magnetopause, because precipitation into the atmosphere occurs during enhanced level of substorm activity.

Fig. 38. Time plots of electron flux and magnetic indeces for the last quarter of 2009.



Selected publication

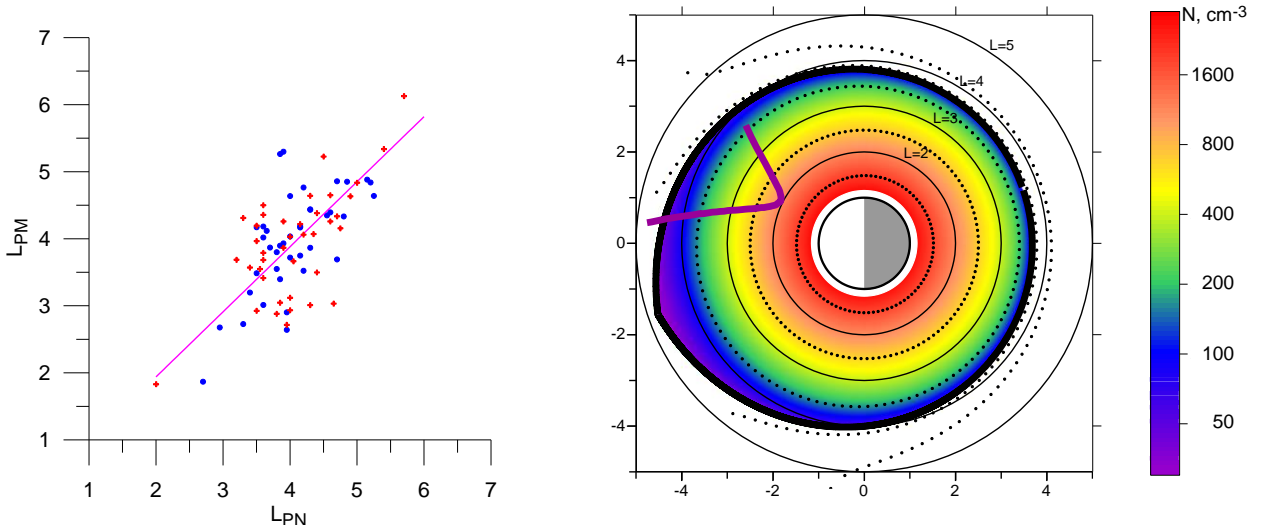
Lazutin, L.L., Dawn-Dusk Asymmetry and Adiabatic Dynamic of the Radiation Belt Electrons During Magnetic Storm, *Advances in Space Research* (2016),
<http://dx.doi.org/10.1016/j.asr.2016.05.047>

Lazutin L.L. Depletion of the outer radiation belt during low activity years
Advances in Space Research, 2017, V. 59, Iss 9, 1 May 2017, Pages 2248–2254, DOI 10.1016/j.asr.2017.02

1.3. Theoretical justification of the method for determining the upper boundary of the terrestrial plasmasphere from experimental data (Russian Academy of Sciences, Space Research Institute)

The previously developed model of the Earth's plasmasphere based on theoretical expressions makes it possible to reconstruct the plasma distribution in the entire plasmasphere from the measurements of one satellite pass and find the position of the last closed plasma stream line L_{PM} . It is shown for the first time that it is this

last closed stream line that coincides with the position of the plasmapause, determined from the experimental data by the Carpenter and Anderson L_{PN} criterion (behind this boundary the plasma density decreases by 5 or more times when the L shell is increased by 0.5). This justifies the reasonability of using such a criterion in comparison with many other formal criteria.



Kotova G.A., Verigin M.I., Bezrukikh V.V., Use of the physically based modeling to choose an adequate method for determining the plasmapause position, Geomagnetism and Aeronomy, 57(4), pp. 375–383, 2017.(Котова Г.А., Веригин М.И., Безруких В.В., Использование физического моделирования для выбора адекватного метода определения положения плазмопаузы, Геомагнетизм и Аэрономия, 57(4), 409-417, 2017.)

1.4. Vertical plasma drifts in the polarization jet band (Russian Academy of Sciences, Space Research Institute)

According to the Doppler measurements on the meridional chain of subaural ionospheric stations in the Yakutsk region, vertical plasma drifts were investigated. For the first time it is shown that in the band of the polarization jet (PJ), fast western plasma drift in the ionospheric F2 layer, plasma flows along the magnetic field lines from the ionosphere to the plasmasphere, and this process determines the ionization losses in the F layer at the phase of the PJ development. Doppler measurements by DPS-4 ionosondes are in agreement with synchronous measurements of plasma drifts on the DMSP satellites during their flight near the Yakutian meridian.

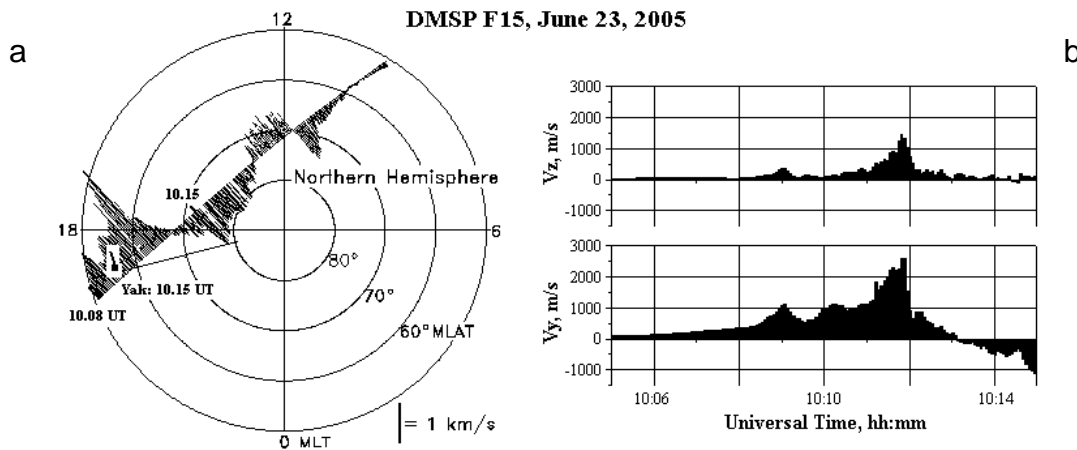


Fig.1. Simultaneous measurements of the plasma drift by the DMSP F-15 satellite during its passage over the Northern Hemisphere and by the digital ionosonde DPS-4 at Yakutsk station: a) variations of the horizontal velocity along the orbit of the DMSP F15 satellite and one horizontal velocity value at the Yakutsk station given as a segment at the time of 10.15 UT (see the inset) in coordinates local magnetic time (MLT) - geomagnetic latitude; b) variations of vertical V_z (top panel) and horizontal V_z (lower panel) of plasma drift velocities according to DMSP F15 satellite data at 10.04-10.16 UT

V. L. Khalipov, A. E. Stepanov, G. A. Kotova, S. E. Kobyakova, V. V. Bogdanov, A. B. Kaisin, and V. A. Panchenko, Vertical plasma drift velocities in the polarization jet observation by ground Doppler measurements and driftmeters on DMSP Satellites, *Geomagnetism and Aeronomy*, Vol. 56(5), pp. 535–544, 2016. (Халипов В.Л., Степанов А.Е., Котова Г.А., Кобякова С.Е., Богданов В.В., Кайсин А.В., Панченко В.А. Вертикальные скорости дрейфа плазмы при наблюдении поляризационного джета по наземным доплеровским измерениям и данным дрейфометров на спутниках DMSP, Геомагнетизм и аэрономия, 56, 568-578, 2016.)

1.5. A new mechanism is suggested of energy transfer from lower energy to higher-energy particles in an ununstable plasma, which takes place under resonant interaction of energetic electrons of the radiation belts with lightning-induced emission.

(Russian Academy of Sciences, Space Research Institute)

The problem of energy exchange between waves and particles, which leads to energization of the latter, in an unstable plasma typical of the radiation belts has been investigated. The ongoing Van Allen Probes space mission brought this problem among the most discussed in space physics. A free energy which is

present in an unstable plasma provides the indispensable condition for energy transfer from lower energy particles to higher energy particles via resonant wave-particle interaction. This process is studied in detail by the example of electron interactions with whistler-mode wave packets originated from lightning induced emission. It is emphasized that in an unstable plasma, the energy source for electron energization is the energy of other particles, rather than the wave energy as is often assumed. The way by which the energy is transferred from lower to higher energy particles includes two processes that operate concurrently, in the same space-time domain, or sequentially, in different space-time domains, in which a given wave packet is located. In the first process, one group of resonant particles with an unstable distribution gives the energy to the wave. The second process consists in wave absorption by another group of resonant particles with a stable distribution, whose energy therefore increases. It is argued that this mechanism represents an efficient means of electron energization in the radiation belts.

Shklyar, D. R. (2017), Energy transfer from lower energy to higher-energy electrons mediated by whistler waves in the radiation belts, *J. Geophys. Res. Space Physics*, 122, 640–655, doi:10.1002/2016JA023263.

1.6. Effect of zero magnetic field, typical for interplanetary space, on cardiovascular system and microcirculation, in the interests of distant space expeditions

(Russian Academy of Sciences, Space Research Institute)

The effects of zero magnetic field conditions on cardiovascular system of healthy adults have been studied. In order to generate zero magnetic field, the facility for magnetic fields modeling “ARFA” has been used. Parameters of the capillary blood flow, blood pressure, and the electrocardiogram (ECG) monitoring were measured during the study. All subjects were tested twice: in zero magnetic field and, for comparison, in sham condition. The obtained results during 60 minutes of zero magnetic field exposure demonstrate a clear effect on cardiovascular system and microcirculation. The results of our experiments can be used in studies of long-term stay in hypo-magnetic conditions during interplanetary missions.

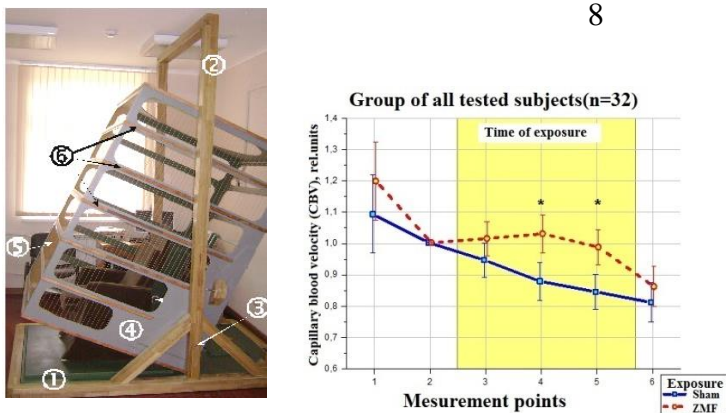


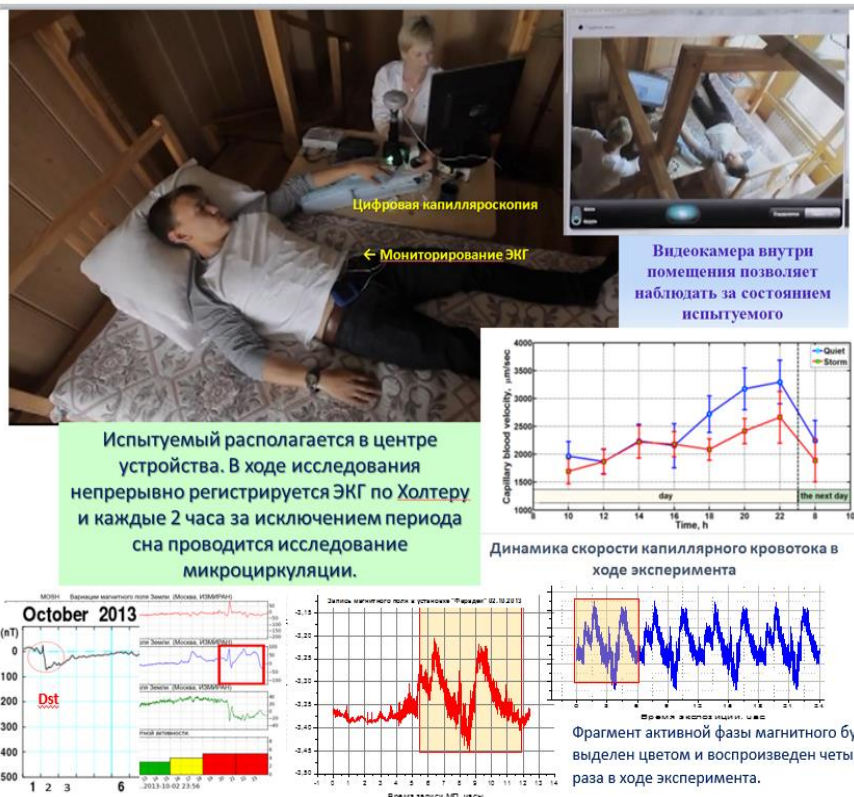
Fig.1 Left: Exposure block of the "ARFA" system. Right - Dynamics of capillary blood flow velocity during the experiment on the effect of the "zero field" (yellow segment) in all studied. The asterisks show the most significant changes.

Yu.I. Gurfinkel, O.Yu. At`kov, A.L.Vasin, T.K.Breus, M.L. Sasonko, R.Yu.Pishchalinikov Effect of zero magnetic field on cardiovascular system and microcirculation, Life Sciences in Space Research, 8 (2016) 1-7.

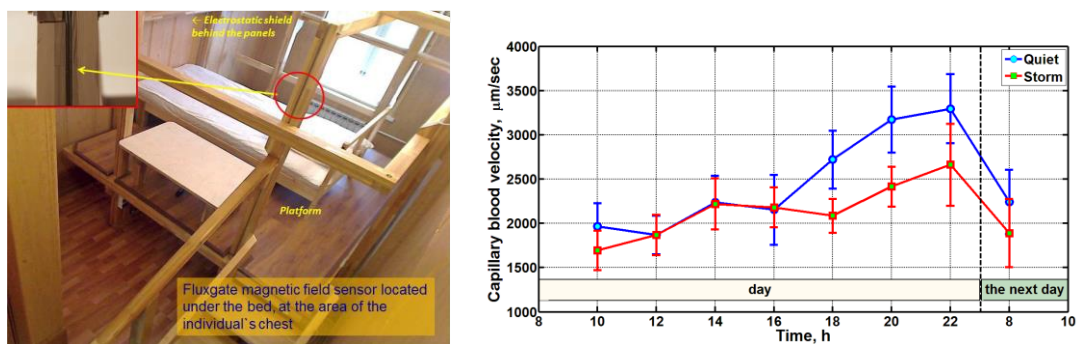
1.7. Geomagnetic storm in laboratory conditions

(Russian Academy of Sciences, Space Research Institute)

For the first time in the world, the medical effects of the geomagnetic storm effect were verified with the help of the Faraday laboratory device simulating magnetic disturbance. On healthy young volunteers with observance of all norms of medical experiment are shown: slowing of capillary blood flow velocity and reduction of heart rate. This result confirms observations *in vivo*, but the regime of the controlled experiment allows to increase the reliability of the results and to conduct research constantly.



Below left: Dst - variation of the magnetic field during the experiment on October 2, 2013, (red square); in the center - the By-component recording (IZMIRAN) of this magnetic storm; on the right - the same magnetic storm reproduced in the Faraday installation.



Left -The Faraday installation, in which volunteers were exposed during a magnetic storm. Right- The dynamics of the capillary blood flow velocity has a significant difference in the period of quiet conditions and during a magnetic storm

Yu I. Gurfinkel, A. L. Vasin, R. Yu. Pishchalinikov, R. M. Sarimov, M. L. Sasonko, T. A. Matveeva Geomagnetic storm under laboratory conditions: randomized experiment. Int J Biometeorology (2017). <https://doi.org/10.1007/s00484-017-1460-8>.

1.8. Remnant Magnetic Fields of Mars and Their Interaction with the Solar Wind

(Russian Academy of Sciences, Space Research Institute)

This work presents a review of studies of the Martian magnetic fields during the early Soviet missions to Mars in 1971–1974, which never approached Mars by closer than 1000 km before the experiment with the Magnetometer/Electronic Reflectometer (MAG/ER) on board the *Mars Global Surveyor* spacecraft, which could descend to altitudes of 80–100 km. At present, the experiment with the magnetometer (MAG) onboard the American *MAVEN* spacecraft adds new data, but the map of distribution of remnant magnetic fields of Mars and the picture of their interaction with the solar wind are already formed and, at its core, obviously, will not be revised. Thus, it would be very instructive to consider the following in detail: (a) what is already known regarding the features and distribution of remnant magnetic fields on Mars; (b) how they control the interaction of solar wind with a weakly magnetized planet (Mars); and (c) what is its distinction from another nonmagnetized planet (Venus).

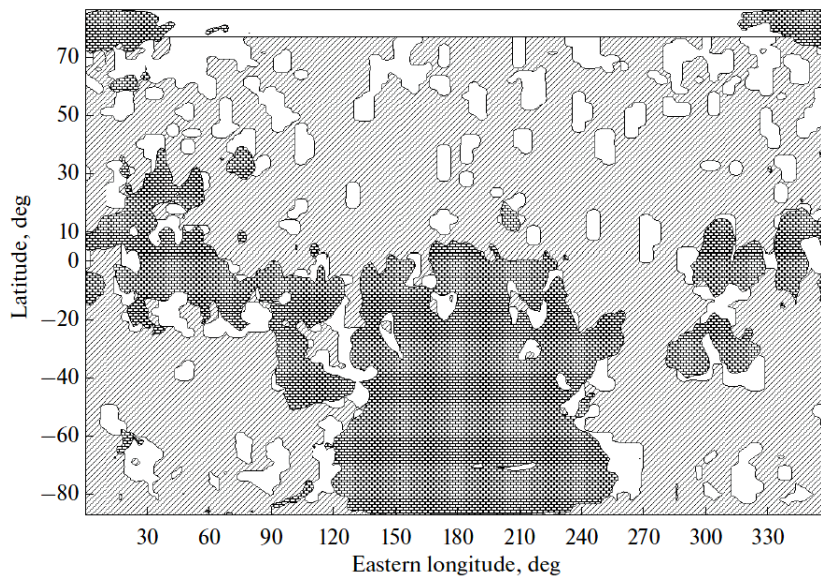


Fig.1. Map of regions on Mars covered by large-scale and small-scale mini-magnetospheres. Large-scale mini-magnetospheres are indicated by brickwise hatching, small-scale mini-magnetosphere are indicated by white regions. Regions outside mini-magnetospheres are shaded.

Breus T. K. and Krymskii A. M., Remnant Magnetic Fields of Mars and Their Interaction with the Solar Wind, *Cosmic Research*, 2017, Vol. 55, No. 4, pp. 235–247.

1.9. Formation of the current sheets in the tail of induced Martian magnetosphere

(Russian Academy of Sciences, Space Research Institute)

An analysis of 80 intervals of the cross-tail Current Sheet (CS) observations by MAVEN spacecraft in the Martian magnetotail revealed the similar features observed in the structure of the Martian and terrestrial CSs:

- 1) the embedding current structures;
- 2) the increase in the CS thickness and the decrease in the current density were observed along with the increase in the value of the magnetic field component perpendicular to the CS plane;
- 3) the spatial scaling of the CS.

The formation of these features is based on the quasiadiabatic dynamics of ions with different masses. Thus, the similar mechanisms of the CS formation operate in the terrestrial and in the induced Martian magnetosphere.

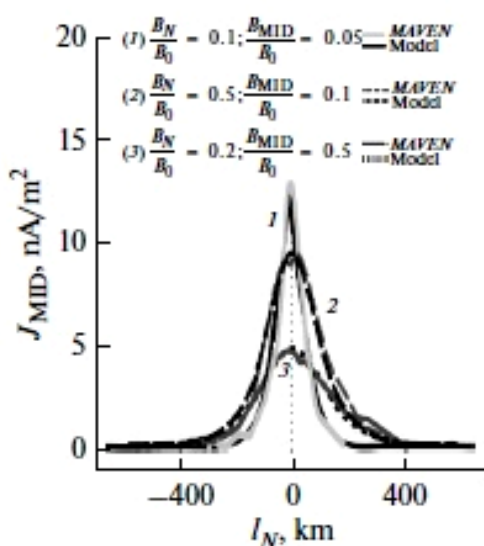


Fig.1 A comparison of the model CS spatial profiles and the CS profiles reconstructed from the MAVEN observations. The profiles are plotted for different values of B_N/B_0 (B_N is the normal magnetic field component in the neutral plane of the CS and B_0 is the value of the magnetic field outside the CS).

References

- 1) Grigorenko E.E., Shuvalov S.V., Malova H.V., Popov V.Yu., Ermakov V.N., Dubinin E., Zelenyi L.M., Structure of the current sheets in the near-Mars magnetotail. MAVEN observations. // Solar System Research, 2017, Vol. 51, No. 5, pp. 347–361.
- 2) Grigorenko E.E., Shuvalov S.V., Malova H.V., Dubinin E., Popov V.Yu., Zelenyi L.M., Imprints of quasi-adiabatic ion dynamics on the current sheet structures observed in the Martian magnetotail by MAVEN // Journal of Geophysical Research. Space Physics. 2017.V.122. doi:10.1002/2017JA024216.

1.10. Electron heating and decrease of proton-to-electron temperature ratio in the magnetotail Plasma Sheet during dipolarizations

(Russian Academy of Sciences, Space Research Institute)

A statistical analysis of 5-year Cluster observations in the magnetotail Plasma Sheet has shown that electrostatic and electromagnetic fluctuations near the electron gyrofrequency contribute in electron heating and transient decreases of proton-to-electron temperature ratio down to 2.0. These fluctuations are usually observed after the dipolarization onset during the interval of cross-tail current reduction and the Bz field enhancement(s) [1].

Reference

- 1) E. E. Grigorenko, E. A. Kronberg, P. W. Daly, N. Yu. Ganushkina, B. Lavraud, J.- A. Sauvaud, L. M. Zelenyi, Origin of low proton-to-electron temperature ratio in the Earth's plasma sheet, *J. Geophys. Res., Space Physics*, 121, doi:10.1002/2016JA022874, 2016.

1.11. Ion leakage at the dayside magnetopause

(Russian Academy of Sciences, Space Research Institute)

Approximation of the magnetosheath ion spectra in the energy range by bi-kappa distributions allows to distinguish two different ion populations – high and low-energetic ions and demonstrate the ion leakage from the magnetosphere to the magnetosheath. Two regimes for the leakage of high-energy (5 – 300 keV) ions across the magnetopause from the magnetosphere to the magnetosheath are selected in strong dependence on the angle (shear) between the magnetosheath magnetic field and the geomagnetic field but not on the interplanetary magnetic field orientation.

The following hypothesis to explain the ion penetration into the magnetosheath from the magnetosphere are suggested:

- a. for high-shear ($>60^\circ$) - ion penetration through thin magnetopause when ion gyroradius is comparable with the magnetopause thickness;
- b. low-shear ($<50^\circ$) - radial diffusion across the thick region of slow change of the magnetic field.

Kirichev, I. P., E. E. Antonova, and M. Stepanova (2017), Ion leakage at dayside magnetopause in case of high and low magnetic shears, *J. Geophys. Res. Space Physics*, 122, doi:10.1002/2016JA023735.

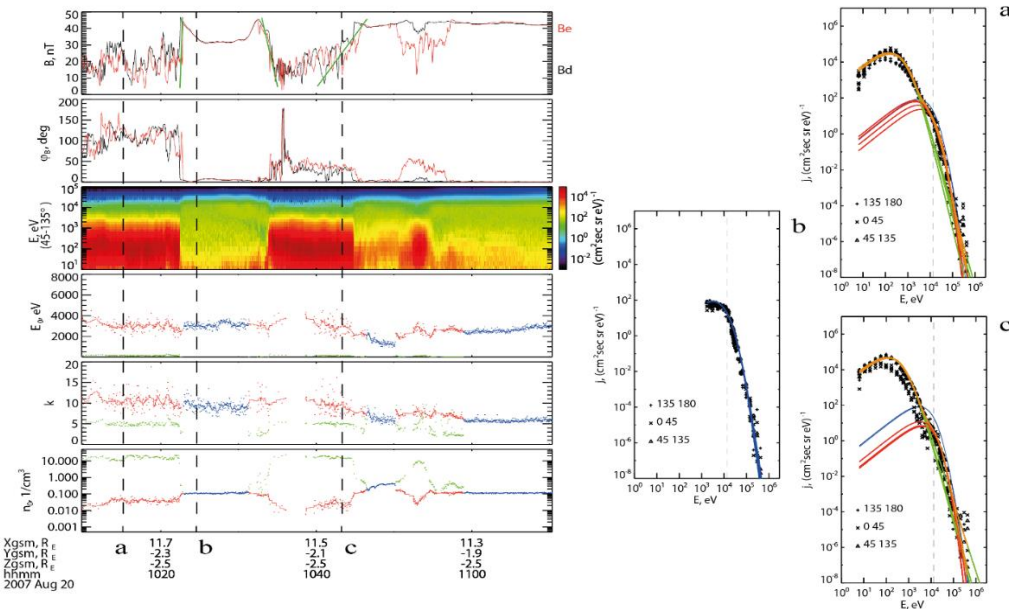


Figure. Left. From top to bottom. The magnetic field measured by the THEMIS-E (red) and THEMIS-D (black) satellites; the magnetic declination angle of the magnetic field, measured by the THEMIS-E (red) and THEMIS-D (black) satellites; the differential ion fluxes measured in the pitch angle interval 45–135°; the characteristic energy; κ and ion number density obtained by fitting the differential ion fluxes with kappa (blue) and bi-kappa (red and green) distributions. All parameters were measured on 20 August 2007. The vertical dashed lines indicate the times of measurement of the spectra shown on right.

Right. Ion differential fluxes in three pitch angle intervals: 0–45° (cross), 45–135° (triangle), 135–180° (plus sign).

(a) Fluxes measured and fitted by a bi-kappa distribution (orange curves) for high-shear. Both high (red) and low (green) energy components are also shown. Blue curves (barely visible and coincident with the red curves) are the same as in (b).

(b) Fluxes measured and fitted by a single kappa distribution inside the magnetosphere for 45–135° pitch angles (four blue curves). (c) Same as on (a) but for low-shear.

1.12. The Results of Venus Studies

(Russian Academy of Sciences, Space Research Institute)

The main corpus of the Venus studies use the data obtained by Venus Express ESA mission. The observations of Venus lasted from 2006 till 2014. Russian contribution to the mission constituted hardware blocks of two science instruments, the infrared channel of SPICAV/SOIR (France/Belgium /Russia), as well as the detectors of PFS Fourier-transform spectrometer. During 2016-2017 the analysis of long-term Venus Express observations was continued.

The analysis of distribution of sulphur compounds in the atmosphere, as well as the other candidates for the UV absorption in the upper cloud deck (Belyaev et al., 2017; Krasnopol'sky 2017, 2018; Luginin et al. 2016; Markiewicz et al. 2018; Vandaële et al 2017ab), water vapour distribution (Fedorova et al., 2016). The studies of the atmospheric dynamics at different altitudes was continued (Gorinov et al., 2018; Khatuntsev et al. 2017), a correlation of the cloud-level air mass movements with the surface altimetry was revealed (Bertaux et al. 2016; Limaye et al 2017). The results were reviews in papers by Koralev 2016; Vandaële et al. 2016.

Also, the studies of the Venus surface, including the preparation for the future space missions involving the descent and landing on Venus were conducted (Ivanov et al. 2017 ab).

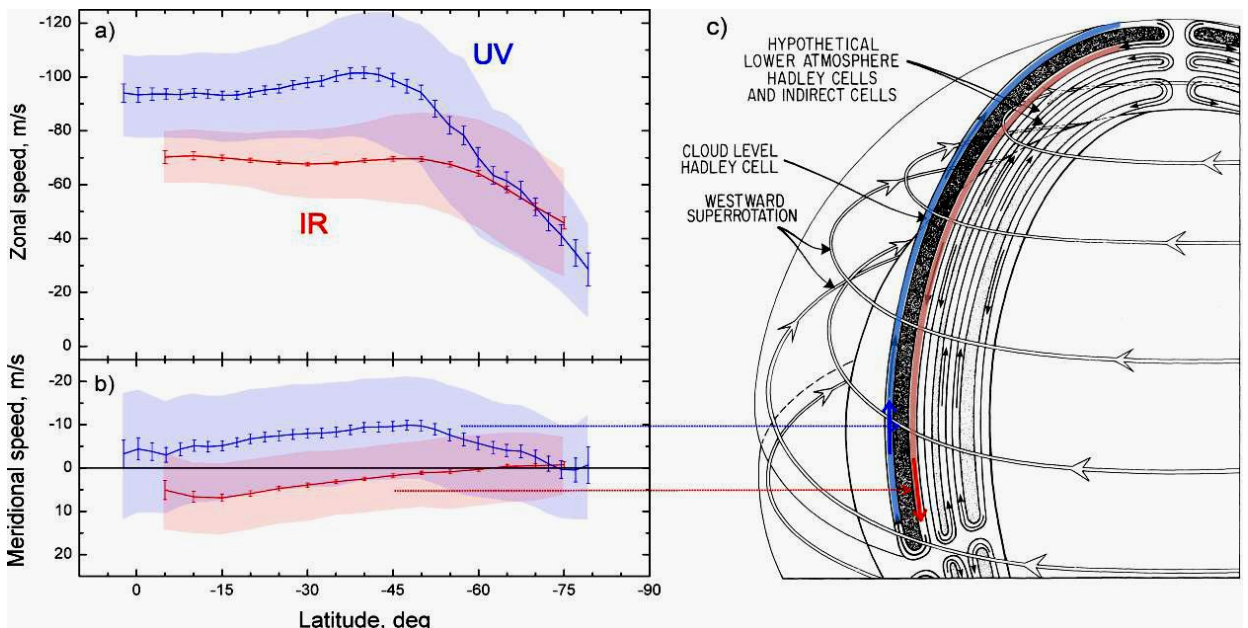


Fig. 1 Mean zonal (a) and meridional (b) latitude wind profiles obtained from the tracking of cloud features. UV data, corresponding to the cloud tops are marked in blue. Near IR data corresponding to the inside of the cloud layer are marked in red. (c) – schematic representation of possible Hadley cells in the Venus atmosphere (Khatuntsev et al., 2017).

1.13. The Results of Mars Studies

(Russian Academy of Sciences, Space Research Institute)

The studies of Mars relied upon observational data of the Mars Express ESA mission. On the 3 of June 2018 Mars Express has celebrated 15 year after the launch. The spacecraft performs science orbital observations from 2004 until now. The science payload includes instruments created with Russian participation, the mapping spectrometer OMEGA, Fourier-transform spectrometer PFS, and the versatile spectrometer SPICAM. Also the data of NASA MAVEN mission were used.

In 2016-2017 diversified studies of the Mars atmosphere dissipation were conducted, in function of the solar activities (Dubinin et al. 2017; Ermakov et al. 2017) or climate factors (Fedorova et al. 2018). Connected studies of Mars aeronomy were completed (Bisikalo et al. 2017; Gerard et al. 2017; Guslyakova et al. 2016; Shematovich et al., 2017ab; Soret et al. 2016). Main climatic cycles of Mars, including the water cycle were characterized (Montmessin et al.

2017 ab). Using the data of imaging instrument geomorphologic studies of the Mars surface were conducted (Bernhardt et al. 2016ab; Ivanov et al. 2017).

Starting from March 2018 the science phase of Trace Gas Orbiter (TGO), the first phase of the ExoMars ESA-Roscosmos mission has begun. The orbiter primarily targets the trace components of the martian atmosphere, possibly pointing to biological or tectonic activities. On board TGO there are two Russian instruments, a spectroscopic suite for the studies of atmospheric chemistry ACS, a collimated neutron detector FREND to map the distribution of the shallow surface water content. Sensitive measurements of the atmospheric gases have been started from 21 April 2018 when the TGO spacecraft began the solar occultation measurements. The first data received during the commissioning phase are being processed, and the planning of future observations is in progress. It is planned that first TGO results will be announced during the EPSC conference in Berlin in September 2018.

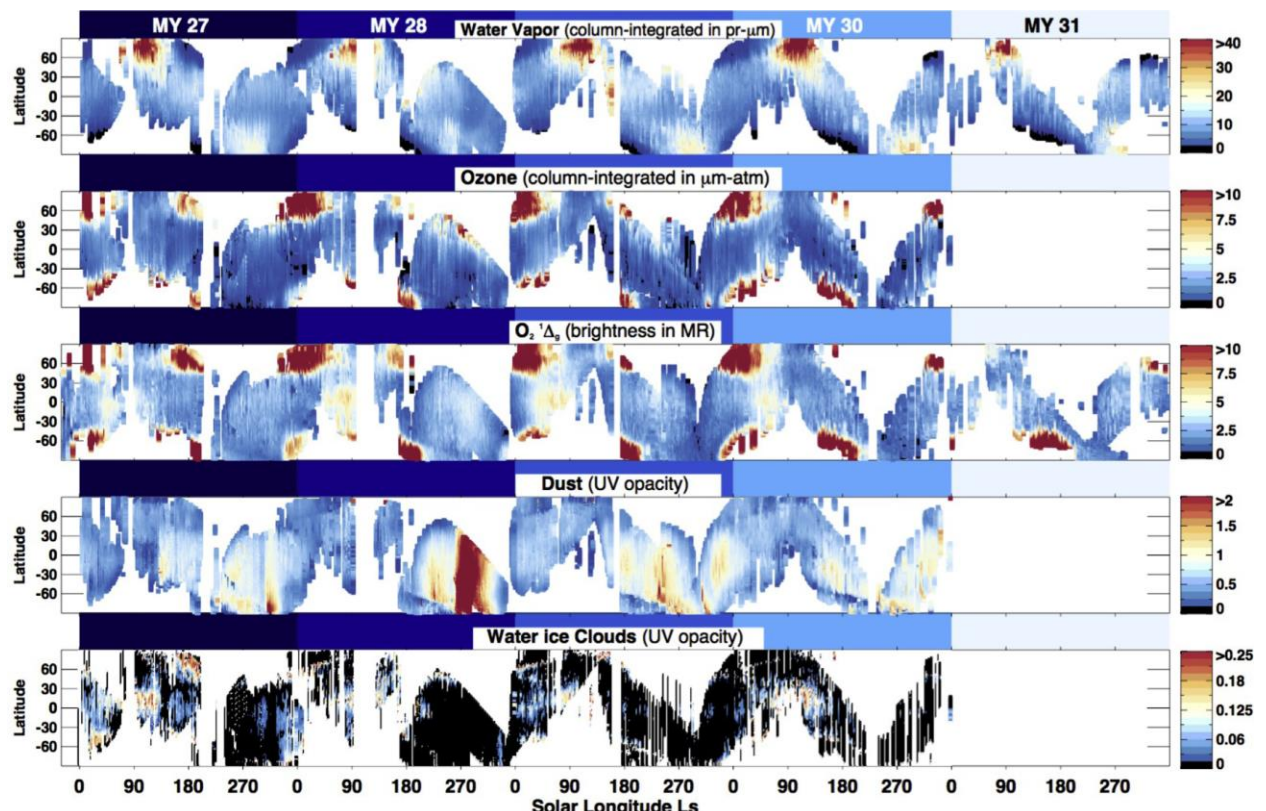


Fig. 2. A compilation of five Martian years of observations by SPICAM/Mars Express in a nadir looking mode. The figure displays zonally averaged values as a function of solar longitude (Ls) of the retrieved (from top to bottom) water vapour, ozone, molecular oxygen singlet delta daytime emission in the near infrared, and dust as well as water ice opacity at 250 nm. The degradation of the UV channel has prevented reliable derivation of ozone and dust/clouds in the ultraviolet during MY31. The unit for each quantity, whose scale is plotted on the right hand-side, is given in brackets.

References

1. Belyaev D. A., D. G. Evdokimova, F. Montmessin, J. L. Bertaux, O. I. Koralev, A. A. Fedorova, E. Marcq, L. Soret, and M. S. Luginin, "Night side distribution of SO₂ content in Venus' upper mesosphere," *Icarus* **294**, 58-71 (2017).
2. Bernhardt H, Reiss D, Hiesinger H, and Ivanov MA. (2016) The honeycomb terrain on the Hellas basin floor, Mars: A case for salt or ice diapirism. *Journal of Geophysical Research (Planets)*, **121**, 714-738.
3. Bernhardt H., H. Hiesinger, M. A. Ivanov, O. Ruesch, G. Erkeling, and D. Reiss,

- "Photogeologic mapping and the geologic history of the Hellas basin floor, Mars," *Icarus* **264**, 407-442 (2016)
4. Bertaux J.-L., I. V. Khatuntsev, A. Hauchecorne, W. J. Markiewicz, E. Marcq, S. Lebonnois, M. Patsaeva, A. Turin, and A. Fedorova, "Influence of Venus topography on the zonal wind and UV albedo at cloud top level: The role of stationary gravity waves," *Journal of Geophysical Research (Planets)* **121**, 1087-1101 (2016).
 5. Bisikalo D. V., V. I. Shematovich, J.-C. Gérard, and B. Hubert, "Influence of the crustal magnetic field on the Mars aurora electron flux and UV brightness," *Icarus* **282**, 127-135 (2017).
 6. Dubinin E., M. Fraenz, M. Pätzold, D. Andrews, O. Vaisberg, L. Zelenyi, and S. Barabash, "Martian ionosphere observed by Mars Express. 2. Influence of solar irradiance on upper ionosphere and escape fluxes," *Planetary and Space Science* **145**, 1-8 (2017).
 7. Ermakov V. N., L. M. Zelenyi, O. L. Vaisberg, E. A. Sementsov, E. M. Dubinin, J. E. P. Connerney, and S. D. Shuvalov, "Initial analysis of ion fluxes in the magnetotail of Mars based on simultaneous measurements on Mars Express and Maven," *Solar System Research* **51**, 335-346 (2017).
 8. Fedorova A., E. Marcq, M. Luginin, O. Koralev, J.-L. Bertaux, and F. Montmessin, "Variations of water vapor and cloud top altitude in the Venus' mesosphere from SPICAV/VEx observations," *Icarus* **275**, 143-162 (2016).
 9. Fedorova A., J.-L. Bertaux, D. Betsis, F. Montmessin, O. Koralev, L. Maltagliati, and J. Clarke, "Water vapor in the middle atmosphere of Mars during the 2007 global dust storm," *Icarus* **300**, 440-457 (2018).
 10. Gérard J.-C., L. Soret, V. I. Shematovich, D. V. Bisikalo, and S. W. Bouger, "The Mars diffuse aurora: A model of ultraviolet and visible emissions," *Icarus* **288**, 284-294 (2017).
 11. D. A. Gorinov, I. V. Khatuntsev, L. V. Zasova, A. V. Turin, and G. Piccioni, "Circulation of Venusian Atmosphere at 90–110 km Based on Apparent Motions of the O₂ 1.27 μm Nightglow From VIRTIS- M (Venus Express) Data," *Geophysical Research Letters* **45**, 2554-2562 (2018).
 12. Guslyakova S., A. Fedorova, F. Lefèvre, O. Koralev, F. Montmessin, A. Trokhimovskiy, and J. L. Bertaux, "Long-term nadir observations of the O₂ dayglow by SPICAM IR," *Planetary and Space Science* **122**, 1-12 (2016).
 13. Ivanov M. A., G. Erkeling, H. Hiesinger, H. Bernhardt, and D. Reiss, "Topography of the Deuteronilus contact on Mars: Evidence for an ancient water/mud ocean and long-wavelength topographic readjustments," *Planetary and Space Science* **144**, 49-70 (2017).
 14. Ivanov M. A., L. V. Zasova, L. M. Zeleny, M. V. Gerasimov, N. I. Ignatiev, O. I. Koralev, and M. Y. Marov, "Estimates of abundance of the short-baseline (1-3 meters) slopes for different Venusian terrains using terrestrial analogues," *Solar System Research* **51**, 87-103 (2017).
 15. Ivanov M. A., L. V. Zasova, M. V. Gerasimov, O. I. Koralev, M. Y. Marov, L. M. Zelenyi, N. I. Ignat'ev, and A. G. Tuchin, "The nature of terrains of different types on the surface of Venus and selection of potential landing sites for a descent probe of the Venera-D Mission," *Solar System Research* **51**, 1-19 (2017).
 16. Khatuntsev I. V., M. V. Patsaeva, D. V. Titov, N. I. Ignatiev, A. V. Turin, A. A. Fedorova, and W. J. Markiewicz, "Winds in the Middle Cloud Deck From the Near-IR Imaging by the Venus Monitoring Camera Onboard Venus Express," *Journal of Geophysical Research-Planets* **122**, 2312-2327 (2017).
 17. Koralev O. I., "Mars and Venus: Different destinies of terrestrial planets," *Herald of the Russian Academy of Sciences* **86**, 285-297 (2016).
 18. Krasnopol'sky V. A., "Annual mean mixing ratios of N₂, Ar, O₂, and CO in the martian atmosphere," *Planetary and Space Science* **144**, 71-73 (2017).
 19. Krasnopol'sky V. A., "Disulfur dioxide and its near-UV absorption in the photochemical

- model of Venus atmosphere," *Icarus* **299**, 294-299 (2018).
20. Krasnopol'sky V. A., "On the iron chloride aerosol in the clouds of Venus," *Icarus* **286**, 134-137 (2017).
 21. Krasnopol'sky V. A., "Sulfur aerosol in the clouds of Venus," *Icarus* **274**, 33-36 (2016).
 22. Krasnopol'sky V. A., and D. A. Belyaev, "Search for HBr and bromine photochemistry on Venus," *Icarus* **293**, 114-118 (2017).
 23. Limaye S. S., S. Lebonnois, A. Mahieux, M. Pätzold, S. Bouger, S. Bruinsma, S. Chamberlain, R. T. Clancy, J.-C. Gérard, G. Gilli, D. Grassi, R. Haus, M. Herrmann, T. Imamura, E. Kohler, P. Krause, A. Migliorini, F. Montmessin, C. Pere, M. Persson, A. Piccialli, M. Rengel, A. Rodin, B. Sandor, M. Sornig, H. Svedhem, S. Tellmann, P. Tanga, A. C. Vandaele, T. Widemann, C. F. Wilson, I. Müller-Wodarg, and L. Zasova, "The thermal structure of the Venus atmosphere: Intercomparison of Venus Express and ground based observations of vertical temperature and density profiles," *Icarus* **294**, 124-155 (2017).
 24. Luginin M., A. Fedorova, D. Belyaev, F. Montmessin, V. Wilquet, O. Koralev, J.-L. Bertaux, and A. C. Vandaele, "Aerosol properties in the upper haze of Venus from SPICAV IR data," *Icarus* **277**, 154-170 (2016).
 25. Markiewicz W. J., E. V. Petrova, and O. S. Shalygina, "Aerosol properties in the upper clouds of Venus from glory observations by the Venus Monitoring Camera (Venus Express mission)," *Icarus* **299**, 272-293 (2018).
 26. Montmessin F., O. Koralev, E. Lefèvre, J. L. Bertaux, A. Fedorova, A. Trokhimovskiy, J. Y. Chaufray, G. Lacombe, A. Reberac, L. Maltagliati, Y. Willame, S. Guslyakova, J. C. Gerard, A. Stiepen, D. Fussen, N. Mateshvili, A. Maattanen, F. Forget, O. Witasse, F. Leblanc, A. C. Vandaele, E. Marcq, B. Sandel, B. Gondet, N. Schneider, M. Chaffin, and N. Chapron, "SPICAM on Mars Express: A 10 year in-depth survey of the Martian atmosphere," *Icarus* **297**, 195-216 (2017).
 27. Montmessin F., M. D. Smith, Y. Langevin, M. T. Mellon and A. Fedorova, Chapter 11: The water cycle; in *The Atmosphere and Climate of Mars* by R. M. Haberle, R. T. Clancy, F. Forget, M. D. Smith, R. W. Zurek (Editors), 820 pp., Cambridge University Press, 2017.
 28. Shaposhnikov D. S., A. V. Rodin, and A. S. Medvedev, "The water cycle in the general circulation model of the martian atmosphere," *Solar System Research* **50**, 90-101 (2016).
 29. Shematovich V. I., "Suprathermal oxygen atoms in the Martian upper atmosphere: Contribution of the proton and hydrogen atom precipitation," *Solar System Research* **51**, 249-257 (2017).
 30. Shematovich V. I., D. V. Bisikalo, J.-C. Gérard, and B. Hubert, "Changes in the Martian atmosphere induced by auroral electron precipitation," *Solar System Research* **51**, 362-372 (2017).
 31. Soret L., J.-C. Gérard, L. Libert, V. I. Shematovich, D. V. Bisikalo, A. Stiepen, and J.-L. Bertaux, "SPICAM observations and modeling of Mars aurorae," *Icarus* **264**, 398-406 (2016).
 32. Vandaele A. C., O. Koralev, D. Belyaev, S. Chamberlain, D. Evdokimova, T. Encrenaz, L. Esposito, K. L. Jessup, F. Lefèvre, S. Limaye, A. Mahieux, E. Marcq, F. P. Mills, F. Montmessin, C. D. Parkinson, S. Robert, T. Roman, B. Sandor, A. Stolzenbach, C. Wilson, and V. Wilquet, "Sulfur dioxide in the Venus Atmosphere: II. Spatial and temporal variability," *Icarus* **295**, 1-15 (2017).
 33. Vandaele A. C., O. Koralev, D. Belyaev, S. Chamberlain, D. Evdokimova, T. Encrenaz, L. Esposito, K. L. Jessup, F. Lefèvre, S. Limaye, A. Mahieux, E. Marcq, F. P. Mills, F. Montmessin, C. D. Parkinson, S. Robert, T. Roman, B. Sandor, A. Stolzenbach, C. Wilson, and V. Wilquet, "Sulfur dioxide in the Venus atmosphere: I. Vertical distribution and variability," *Icarus* **295**, 16-33 (2017).
 34. Vandaele A. C., S. Chamberlain, A. Mahieux, B. Ristic, S. Robert, I. Thomas, L.

Trompet, V. Wilquet, D. Belyaev, A. Fedorova, O. Koralev, and J. L. Bertaux,
 "Contribution from SOIR/VEX to the updated Venus International Reference
 Atmosphere (VIRA)," Advances in Space Research **57**, 443-458 (2016).

1.14. Empirical ionospheric trough model for the daytime winter conditions.
 (Russian Academy of Sciences, Pushkov Institute of Terrestrial Magnetism,
 Ionosphere and Radio Wave Propagation (IZMIRAN))

For the first time, an empirical model of the daytime ionospheric trough under quiet winter conditions ($K_p = 2$) was constructed for an arbitrary level of solar activity in the Northern and Southern hemispheres. It consists of a trough position model and a trough shape model, which is the latitude-longitude f_0F2 variation in the geographic latitude range of 40-85° in both hemispheres. In fact, we are dealing with an f_0F2 model in the winter daytime high-latitude ionosphere. The f_0F2 model is valid for November-February in the North hemisphere and for May-August in the South hemisphere, although the trough may be unobservable around the noon under the conditions of high solar activity. The model is based on the Intercosmos-19 and CHAMP satellite data. The model was used to reveal and study in detail the diurnal and longitudinal variations in the trough minimum position. The latitudinal and longitudinal variations in f_0F2 were also identified and investigated. It was shown that the constructed model reproduces the f_0F2 diurnal, longitudinal, and latitudinal variations more adequately than the international model ionosphere IRI-2016. For example, Fig.1 shows longitudinal variations in the trough position for 12 LT in the North and South hemispheres. The model is available on the IZMIRAN website: <http://www.izmiran.ru/ionosphere/sm-mit/>.

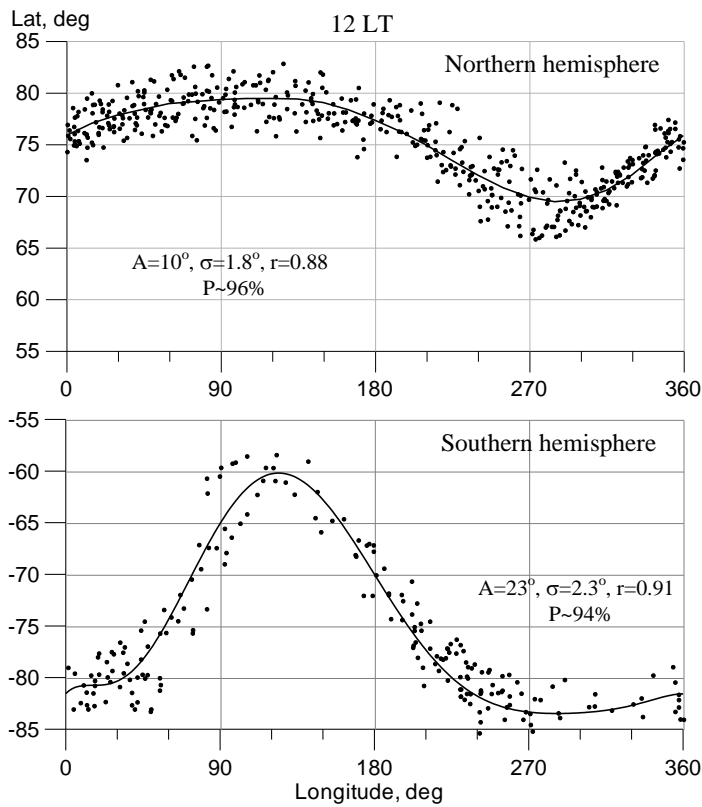


Figure 1. Longitudinal variations in the midday trough position f (11: 00-13: 00 LT) under low solar activity (LSA) in the North and South hemispheres as inferred from Interkosmos-19 and CHAMP data. Shown are the amplitude A , standard deviation σ , correlation coefficient r , and occurrence probability P .

Karpachev A.T., Klimenko M.V., Klimenko V.V., Pustovalova L.V. Empirical model of the main ionospheric trough for the nighttime winter conditions. // J. Atmos. Sol-Terr. Phys. v.146, pp.149–159. doi:10.1016/j.jastp.2016.05.008. 2016.

1.15. Longitudinal variations in the ionospheric trough position

(Russian Academy of Sciences, Pushkov Institute of Terrestrial Magnetism, Ionosphere and Radio Wave Propagation (IZMIRAN))

For the first time, longitudinal variations in the position of the winter ionospheric trough were revealed and investigated as a function of *geomagnetic latitude* at all hours LT in the North and South hemispheres for both high (HSA) and low (LSA) solar activity conditions. The Kosmos-900, Interkosmos-19, and CHAMP satellite data obtained under quiet geomagnetic conditions ($K_p = 2$) were used. The amplitude of the longitudinal effect (LE) in the ionospheric trough position was greater in the daytime ($7\text{-}8^\circ$) than at night ($4\text{-}5^\circ$). The average LE amplitude reached a maximum of 16° in the South hemisphere at 08:00 LT under HSA in the daytime and 6° at 06:00 LT under LSA, at night. On separate days, the nighttime LE amplitude can reach $9\text{-}10^\circ$. The shape of the longitudinal effect in the North and South hemispheres is fundamentally different. In the South hemisphere, the longitudinal effect can be approximately described by the first-order harmonic,

while in the North hemisphere the second-order harmonic also appears at night. The cause of longitudinal variations in the ionospheric trough position is discussed in terms of the GSM TIP model. The model calculations show that at low solar activity, LE in the position of the daytime trough is mainly determined by the longitudinal variation in the ionization function due to the longitudinal variations in the solar zenith angle and distribution of the atomic oxygen density. LE in the nighttime trough position is due to the ionization of precipitating auroral particles, composition of the neutral atmosphere, and electric field. For example, Fig. 1 shows longitudinal variations in the trough position in the North hemisphere.

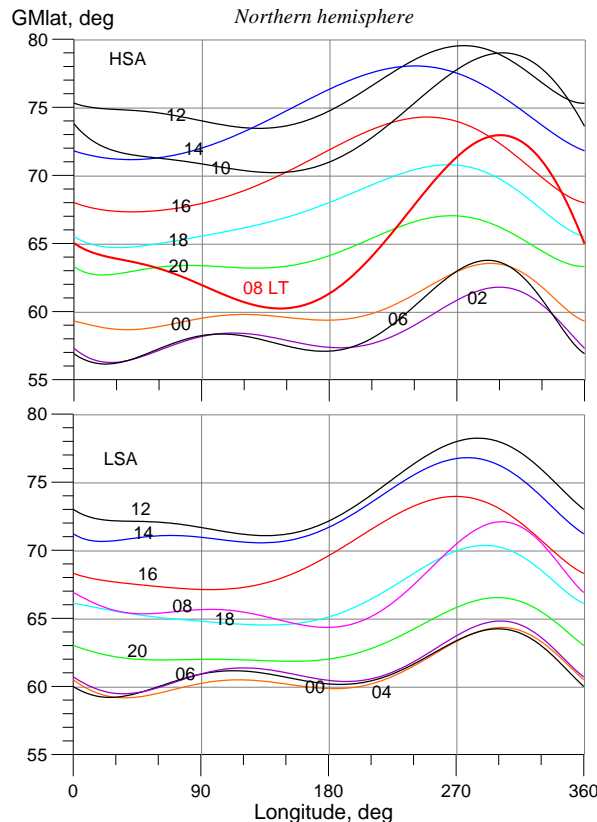


Fig. 1. Longitudinal variation in the trough position at different hours LT in the North hemisphere for HSA (top) and LSA (bottom).

Karpachev A.T., Klimenko M.V., Klimenko V.V. Longitudinal variations in the ionospheric trough position // Advances in Space Research, 2018 (submitted).

1.16. A new global model of the total atmosphere (EAGLE)

(Russian Academy of Sciences, Pushkov Institute of Terrestrial Magnetism, Ionosphere and Radio Wave Propagation (IZMIRAN))

A new model atmosphere (EAGLE) was developed, which allows interactive .5 of the state of the entire atmosphere system including the troposphere, stratosphere, mesosphere, thermosphere, and ionosphere-plasmasphere. It consists of the HAMMONIA chemistry and climate model for atmospheric processes in the

altitude range from the Earth surface up to 80 km and the GSM TIP model for the altitudes from 120 km to the upper boundary (about 15 Earth radii). In the 80-120 km region, the temperature and density fields from the HAMMONIA model are used in the GSM TIP model to calculate the circulation, thermosphere composition, behavior of the ionosphere, and electrodynamics. The influx of nitrogen oxides, ion drag and Joule heating values from GSM TIP are used in the HAMMONIA model. The tests have shown that the EAGLE model reproduces the low temperatures in the polar summer mesosphere better than the GSM TIP model alone. The EAGLE model will be applied to investigate how the solar activity (solar protons, solar flares, high-energy electrons, geomagnetic disturbances, etc.) and the meteorological disturbances in the lower atmosphere (sudden stratospheric warming, cyclonic activity, and restructuring of the atmospheric circulation associated with possible climate changes) can affect the state of the thermosphere-ionosphere system. As shown in Figure 1, the monthly mean temperature for January 2009 calculated with the EAGLE model agrees qualitatively with the MIPAS observation data.

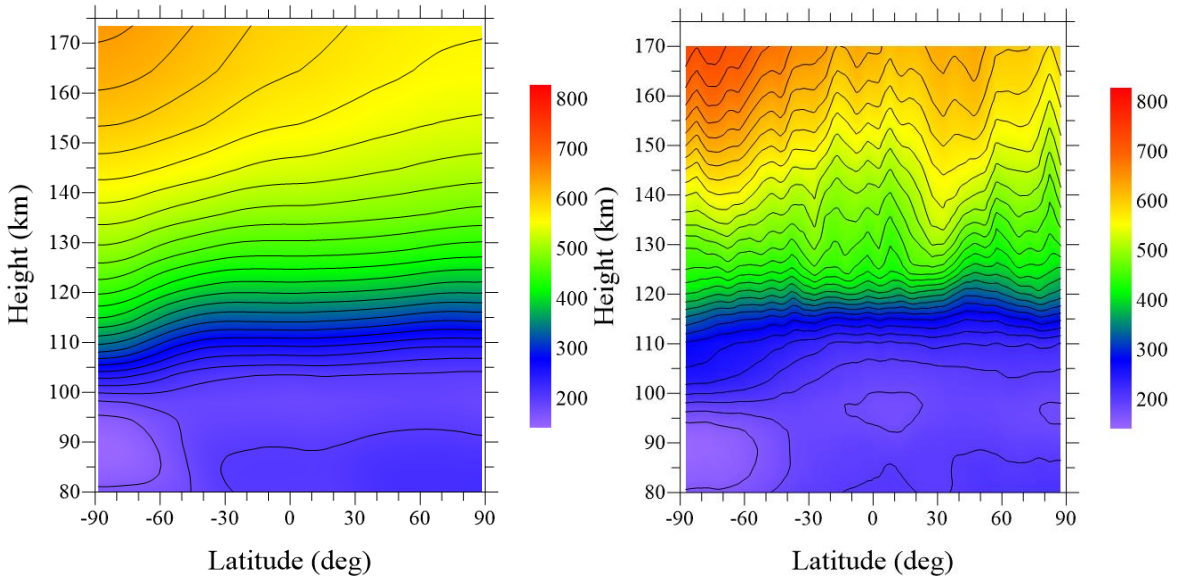


Figure 1. Latitude-altitude distribution of the neutral temperature (K) averaged in longitude and time for January 2009 as derived from HAMMONIA model calculations (left panel) and MIPAS observations (right panel).

The temperature anomalies in the altitude range of 0 - 80 km during the stratospheric warming in 2009 according to the HAMMONIA model calculations also show a good agreement with MIPAS observations (see Figure 2).

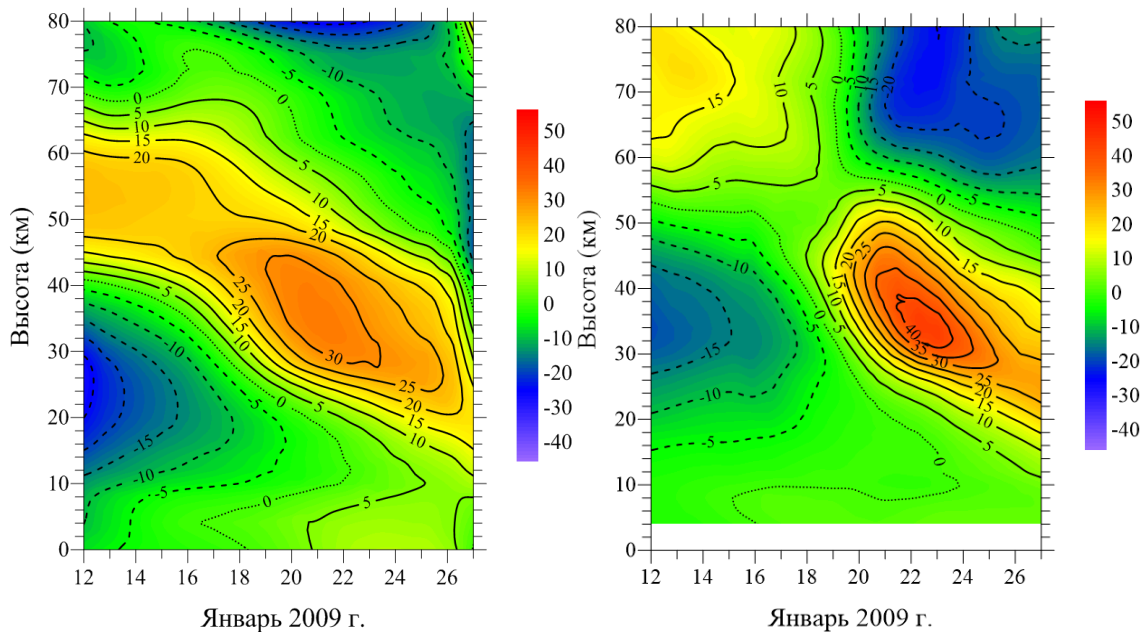


Figure 2. Time variations in the vertical distribution of the zonal-mean polar temperature anomalies (latitudes of 70-90°N) in the altitude range of 0-80 km in the period of the stratospheric heating of 2009 as inferred from MIPAS observations (left) and HAMMONIA model (right).

Klimenko, M. et al. Ionospheric effects of the sudden stratospheric warminenin of 2009: results of the first version of the EAGLE model. Submitted to Chemical Physics.

1.17. Experimental study of the direct plasma heating process in the solar corona (primary energy release) based on data of the corona observations in MgXII 8.42 Å line

(Russian Academy of Sciences, Lebedev Physical Institute (FIAN))

Study of experimental dependence of emission measure (or similar characteristics) of solar flares on flow and intensity of magnetic field in the flare area concerning earlier unexplored area A0.01 - B1.0 (on GOES scale) was performed and published in 2016-2017 based on the data obtained from TESIS space experiment conducted on CORONAS-Photon spacecraft. Plasma heating process at early stages of flare events was studied by a number of authors, however, only for large flares - from X-ray class A and higher. These studies showed logarithmic dependence between X-ray class of a flare and the flare plasma temperature. The studies showed that a power-law relationship exists between X-ray class and emission measure. Herewith, no progress has been made in any study towards the flares weaker than A1 flares.

The major problem of earlier revealed dependencies was that their extrapolation predicted absence of plasma heating in the flares lower than A1. Yet, LPI RAS observed plasma heating in flares of a far lower level based on THESIS data. Thus, a raw hypothesis appeared that plasma heating at early (impulsive)

phase of small flares (microflares) is subject to a dependence other than that revealed earlier for medium and large events.

The purpose of the study was to obtain data on plasma heating at early stages of low class flares (lower than A1.0). A history of plasma heating in the events registered by TESIS in April 2009, during the phase of low solar activity, was collected for this purpose. More than 400 flares were processed in total, which made it possible to obtain consistent statistical results. Two-temperature approximation was used for the calculation of temperature. Herewith, the colder component was identified with background plasma and the hotter component was identified with the flare itself.

A range of significant results was obtained as a result of the study. First, it was shown that logarithmic dependence between X-ray class of a flare revealed during earlier studies was imaginary and was associated with a limited group of events. The full group (from the lowest to the highest classes) showed that general dependency is of power law nature. This conclusion is essential for a number of fundamental issues of solar physics, including the issue of total thermal energy released in solar flares. Second, the minimal X-ray class of a flare at which plasma heating may occur at initial stage thereof was first determined as class A0.0002. Third, dependences of plasma temperature on characteristics of magnetic field in the flare area were determined for the first time for solar microflares.

The results of the study were published in the following two papers:

Kirichenko, A. S.; Bogachev, S. A., Plasma Heating in Solar Microflares: Statistics and Analysis, *The Astrophysical Journal*, Volume 840, Issue 1, article id. 45, 8 pp. (2017)

Kirichenko, A. S.; Bogachev, S. A., The Relation Between Magnetic Fields and X-ray Emission for Solar Microflares and Active Regions, *Solar Physics*, Volume 292, Issue 9, article id. 120, 15 pp. (2017)

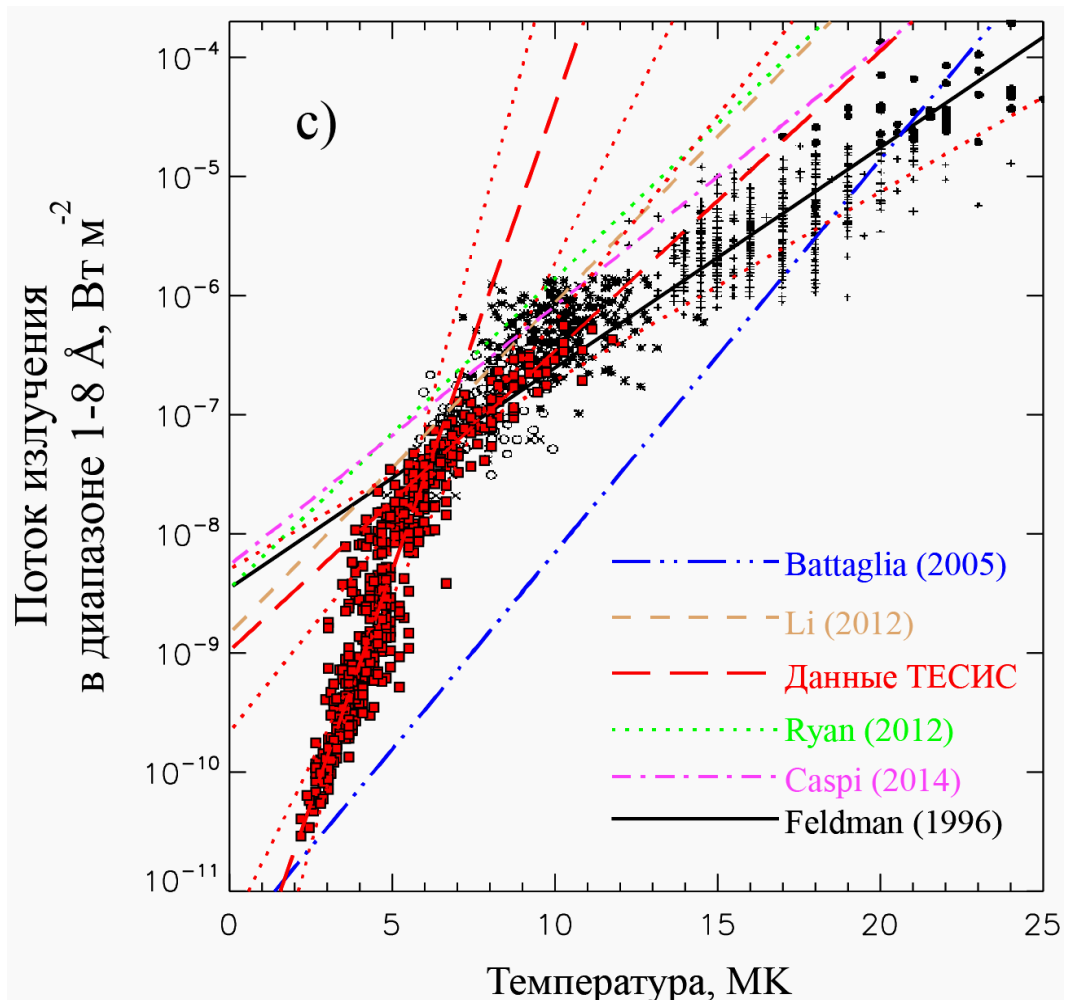


Figure 1.1 Revised dependence of emission flow in 1-8 Å band on plasma temperature.

1.18. Topological studies of large coronal mass ejections within the altitudes band from 0 to 2 solar radii

(Russian Academy of Sciences, Lebedev Physical Institute (FIAN))

Large coronal mass ejections are mainly observed by solar coronagraphs starting from the distance of 2 solar radii and farther (closer areas are hidden by artificial moon of the coronagraph). As a rule, an already formed emission comes into view at such distances. Consequently, the process of its formation is hidden and, therefore, unexplored.

The results of the study of an unusual coronal ejection, at the early stage of which a complex pattern of ejection acceleration was detected being supposedly indicative of the fact that the ejection had been formed by several different mechanisms, were prepared and published in 2016-2017 based on THERESIS space experiment data obtained in CORONAS-Photon spacecraft. The event took place on April 23, 2009 and included two impulsive acceleration phases as well as an impulsive deceleration phase. The first acceleration phase was identified as

flexural instability frequently observed in the breakout model. In other words, the magnetic field of ejection had an appearance of a twisted tube, which unwound during relaxation resulting in initial movement of the matter. Additional acceleration impulse was gained through flow of some matter from top to bottom of the tube resulting in decreased mass and, accordingly, in increased ejection speed. The second acceleration impulse was gained through magnetic reconnection - interaction with magnetic fields opposite in sign. Deceleration impulse was explained by interaction between the studied ejection and earlier ejected matter - new ejection reached the previous one and decelerated (herewith, the second ejection accelerated on the contrary).

Therefore, the paper managed to describe quite a complex event of ejection movement at the early stage being considerably different from standard models. Supposedly, in future such observations may promote enhanced accuracy of ejection movement models in the Sun-Earth system.

The results of the study were published in the following paper:

A.A. Reva, A.S. Kirichenko, A.S. Ulyanov, and S.V. Kuzin, Observations of the coronal mass ejection with a complex acceleration profile, The Astrophysical Journal, Volume 851, Issue 2, article id. 108, 15 pp. (2017)

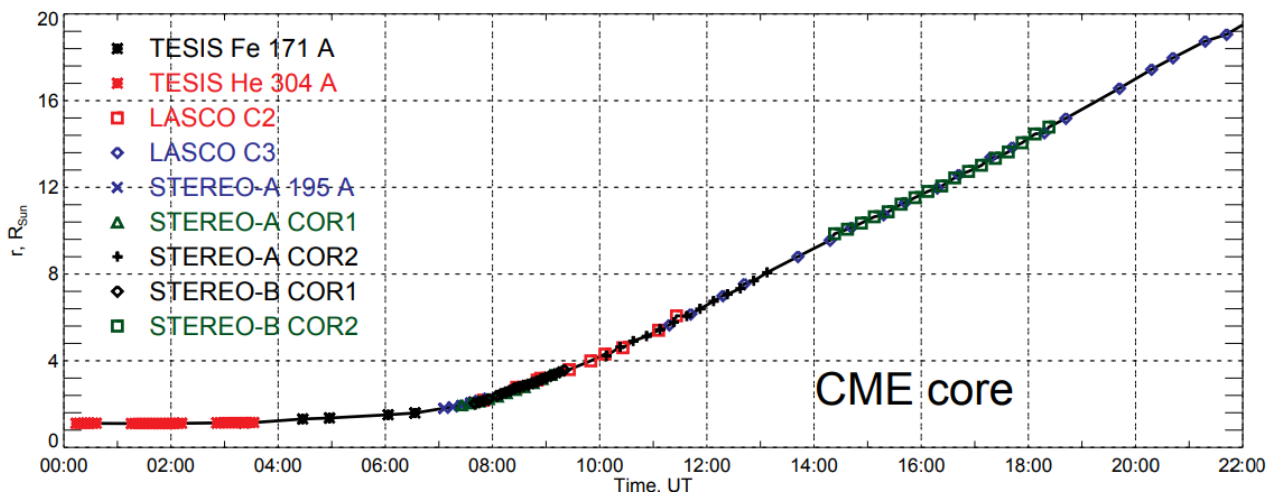


Figure 1.2 Time variation of CME core distance from the Sun. Measurement unit: solar radius

1.19. It has been obtained experimental confirmation of the theoretical hypothesis that some auroral forms in the vicinity of magnetospheric cusp and on the polar edge of the auroral oval are related with magnetic reconnection in near-Earth space. The reconnection in the development of the magnetospheric substorm is traditionally regarded as an important link, which ensures the influx of energy from the interplanetary medium into the magnetosphere and its explosive release in the magnetospheric tail. The result

shows that high-latitude optical observations can effectively complement the tools for studying and monitoring of space weather formation processes.
 (Russian Academy of Sciences, Kol'skiy Scientific Center, Polar Geophysical Institute)

Publications:

- 1) Kornilov I.A., Kornilova T.A., Golovchanskaya I.V. Relationship between auroral oval poleward boundary intensifications and magnetic field variations in the solar wind // Geomagnetism and Aeronomy. 2016. T. 56. № 3. C. 268-275.
- 2) Safargaleev V.V., Mitrofanov V.M., Roldugin A.V. Simultaneous optical and satellite observations of auroras in the mantle: Case study // Geomagnetism and Aeronomy. 2016. T. 56. № 6. C. 706-715.

1.20. Using the data from four NOAA POES spacecraft on the precipitation of >1 MeV electrons as well as electrons and protons of lower energies the conclusion on different mechanisms of the relativistic electron precipitation (REP) from the radiation belt is made. One of the mechanisms is the scattering of the relativistic electrons in the magnetic field with the large curvature of field lines. Others are related to scattering by different kinds of waves. It is shown that a fraction of REP, which are not related to waves, is 20-30%. The fraction of REP related to electromagnetic ion cyclotron (EMIC) waves, which are commonly suggested as one of the main REP mechanism, is only 15-20%.

(Russian Academy of Sciences, Kol'skiy Scientific Center, Polar Geophysical Institute)

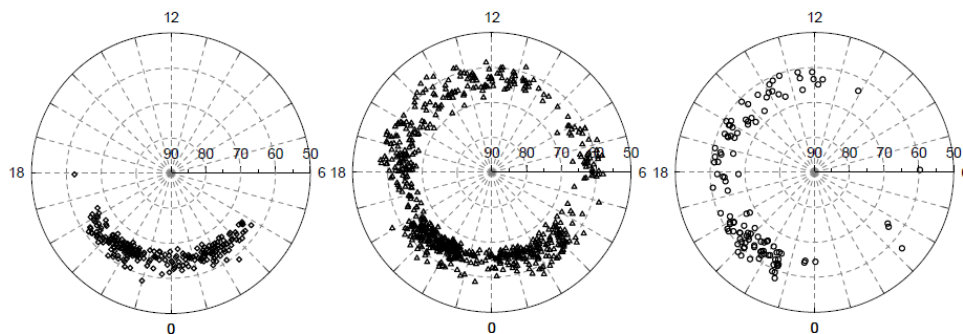


Figure 9. Spatial distribution of REP events constructed on the basis of NOAA POES data. On the left - the events, which are not related to the wave activity; in the middle - REP events related to interaction of relativistic electrons with plasmaspheric hiss or UHR waves; on the right - REP events related to interaction of relativistic electrons with EMIC waves.

Publications:

- 1) Yahnin A.G., T.A. Yahnina, N.V. Semenova, B.B. Gvozdevsky and A.B. Pashin (2016), Relativistic electron precipitation as seen by NOAA POES, *J. Geophys. Res. Space Physics*, 121, doi:10.1002/2016JA022765.
- 2) Yahnin A.G., T.A. Yahnina, N.V. Semenova, A.B. Pashin (2016), Morphology of the relativistic electron precipitation. Proceedings of the V International conference "Atmosphere, Ionosphere, Safety" Kaliningrad June 19-25, 2016 // -Kalininograd, Russia: Immanuil Kant Baltic Federal University, 2016. P. 507-513.

1.21. The numerical modeling shows that horizontal inhomogeneities of the ionosphere are rising after precipitation of high-energy protons cause bursts of wave impedance detected in the geophysical observatory Lovozero.
 (Russian Academy of Sciences, Kol'skiy Scientific Center, Polar Geophysical Institute)

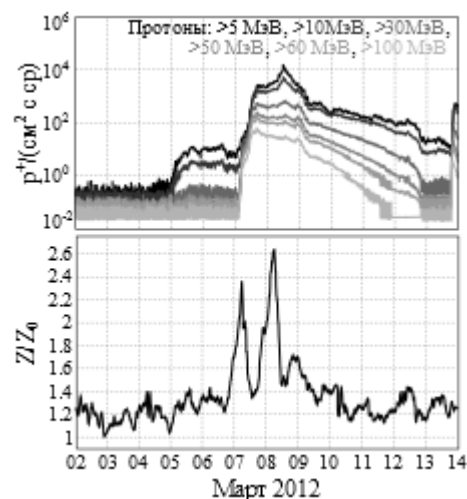


Figure 10. A proton flux (GOES-15) and a normalized wave impedance Z/Z_0 in obs. Lovozero during solar proton events in March 2012

1.22. Acceleration of Electrons in Solar Flares

(Russian Academy of Sciences, Institute of Applied Physics,
 Russian Academy of Sciences, Pulkovo Observatory)

Two mechanisms of electron acceleration in solar flares are proposed. The first one occurs in solar magnetic loops in the course of electric current oscillations [1]. The magnetic loop is presented as an RLC-circuit with the electric current generated by convective motions in the photosphere. Eigen-oscillations of the electric current in a loop induce an electric field directed along to the loop axis. It is shown that sudden reductions in type IV and pulsating type III solar radio bursts

provide evidences in favor of electron acceleration in coronal loops. Energization rate, $\approx 3 \times 10^{33} eV s^{-1}$, and the energy of accelerated electrons, 30-100 keV, were estimated. It is shown that this acceleration mechanism can work also in the course of the 5-min photospheric oscillations.

The second, more powerful acceleration mechanism is driven by the magnetic Rayleigh-Taylor instability which develops at the loop foot-points in the chromosphere [2]. It is shown that for a sufficiently strong electric current, $I_0 \geq 10^{10}$ A, the electrical current pulse propagates in the nonlinear mode and generates a strong longitudinal electric field E_z , which strongly depends on the current $E_z \propto I_0^3$ and can exceed the Dreicer field ($E_z > E_D$). In this case, the bulk of electrons in the site of the current pulse is in a runaway mode, and the energy release rate in the chromosphere increases significantly. The electric field at the pulse edge can exceed the Dreicer field starting from the chromosphere level with the number density $n \approx 10^{13} \text{ cm}^{-3}$. At a lower current $I_0 < 10^{10}$ A, a super-Dreicer mode at the higher levels of the chromosphere with $n < 10^{12} \text{ cm}^{-3}$ occurs (Figure 1). This is the way to the solution of the long-standing “number problem” in the physics of solar flares.

References

1. Zaitsev V.V. and Stepanov A.V.: Acceleration and Storage of Energetic Electrons in Magnetic Loops in the Course of Electric Current Oscillations // 2017, Solar Physics, **292**, 141-152. DOI: [10.1007/s11207-017-1168-2](https://doi.org/10.1007/s11207-017-1168-2).
2. Zaitsev, V.V., Kronshtadtov, P.V. and Stepanov, A.V.: Rayleigh-Taylor Instability and Excitation of Super-Dreicer Electric Fields in the Solar Chromosphere // 2016, Solar Physics, **291**, No 11, pp.3451-3459. DOI: [10.1007/s11207-016-0983-1](https://doi.org/10.1007/s11207-016-0983-1).

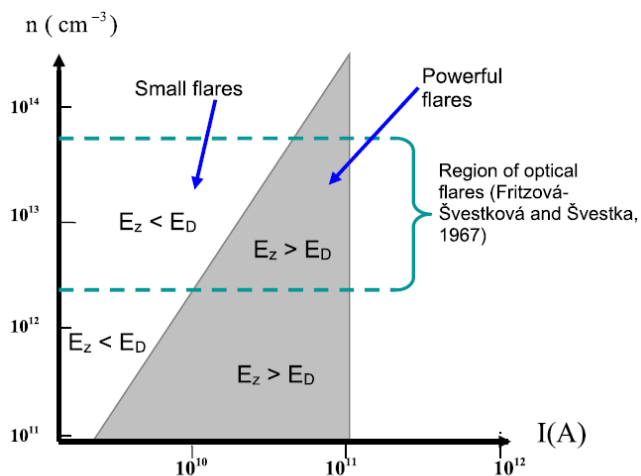


Figure 1. Diagram ‘plasma density vs. electric current’ for typical solar flare loop. The regions of sub-Dreicer and super-Dreicer (in grey) electric fields formed at the leading edge of the current pulse propagating along magnetic loop away from the Rayleigh-Taylor instability domain are shown.

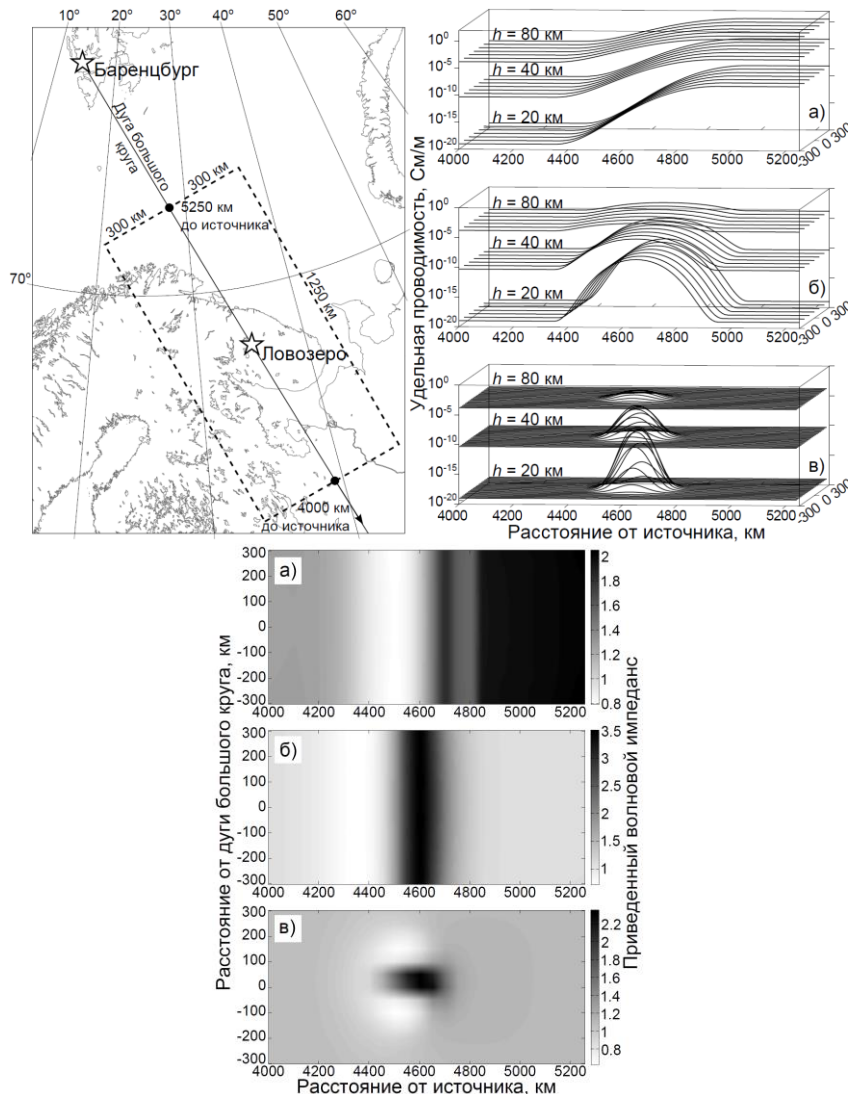


Figure 11. On the left: location of part of the calculation region (dashed curve) relative to the electromagnetic field registers. On the centre: distributions of the ionospheric conductivity at heights of 20, 40, and 80 km of the part of the calculation region. On the right: distribution of the reduced wave impedance Z/Z_0 near the Earth's surface. The types of irregularities: (a) transition region, (b) shaft, and (c) funnel.

Authors: Larchenko A. V., Lebed' O. M., Fedorenko Yu. V., Pil'gaev S. V.

Publication:

Lebed' O. M., Larchenko A. V., Pil'gaev S. V., Fedorenko Yu. V. Reaction of the High-Latitude Lower Ionosphere to Solar Proton Events From to Observations in the ELF Range // Geomagnetism and Aeronomy, Pleiades Publishing, Ltd., 2017, Vol. 57, No. 1, pp. 51–57.

1.23. 27-variations of galactic cosmic rays with PAMELA and ARINA (National Research Nuclear University “MEPhI”)

Temporal variations of galactic cosmic ray (GCR) flux with a period of about 27 days were firstly discovered by S. Forbush based on measurements of the World Network of Ionization Chambers created in the late 1930s (they were a prototype of a modern Neutron monitors) [1, 2]. Later in the 1960s, the first measurements of the GCR fluxes in the outer space were carried out and they confirm this result [3]. The subsequent analysis showed the connection of 27-day variations in the flux of galactic particles with the interplanetary medium characteristics like solar wind speed or intensity of the interplanetary magnetic field, which is related to the rotation of the Sun around its axis having a similar period. However, a complete physical description of the effect is not currently available due to a limited statistics and the accuracy of available observations.

Today we made a new step in our understanding of 27-day variations of GCR fluxes. A famous magnetic spectrometer PAMELA [4] and scintillator spectrometer ARINA [5] are carried out onboard a Russian satellite Resurs-DK1 during an almost full solar cycle from June 2006 up to January 2016. Some extremely important scientific results were obtained with PAMELA experiment. Mostly they are connected with the primary cosmic radiation, in particular, with the fluxes of antiparticles (positrons and antiprotons), which are associated with the study of properties of "dark" matter. A new kind of information was obtained with ARINA experiment, mostly about particles in the radiation belt, in particular, about their perturbations related to the geophysical nature.

PAMELA and ARINA experiments carried out precise measurements of cosmic ray fluxes over a wide range of energies complementing the energy interval from 30 MeV to 20 GeV in which practically no experimental data were available although this range is the most interesting for study of 27-day variations of the GCR. Due to the scientific information from these devices, it becomes possible to obtain a new information on the changes in the period and phase of GCR flux variations, as well as the amplitudes depending on the energy (rigidity) of the particles.

A daily data about fluxes of galactic protons and helium for different rigidities were obtained during processing of PAMELA and ARINA information. Based on methods of harmonic analysis we found five cases of 27-day variations of GCR fluxes during all the time of operation of instruments. The most interesting case for exploration was in January 2007 – October 2008 associated with the long low level of solar activity and practically flat heliospheric current sheet. These conditions led to the formation of a continuous stationary periodic signal in the GCRs flux.

Figure 1 shows the dependence of the maximum amplitude of the variations on the particle rigidity obtained from the PAMELA and ARINA experiments. A single power law cannot describe the dependence for all energies as predicted by theoretical models [6]. Today it has been shown that only at rigidities above \sim one GV

the dependence really confirm a power law. For the rigidities from 0.3 to 0.7 GV, the deviation from the theory was firstly discover with decreasing the rigidity of the particles, the amplitude rapidly decreases and the oscillations practically disappear.

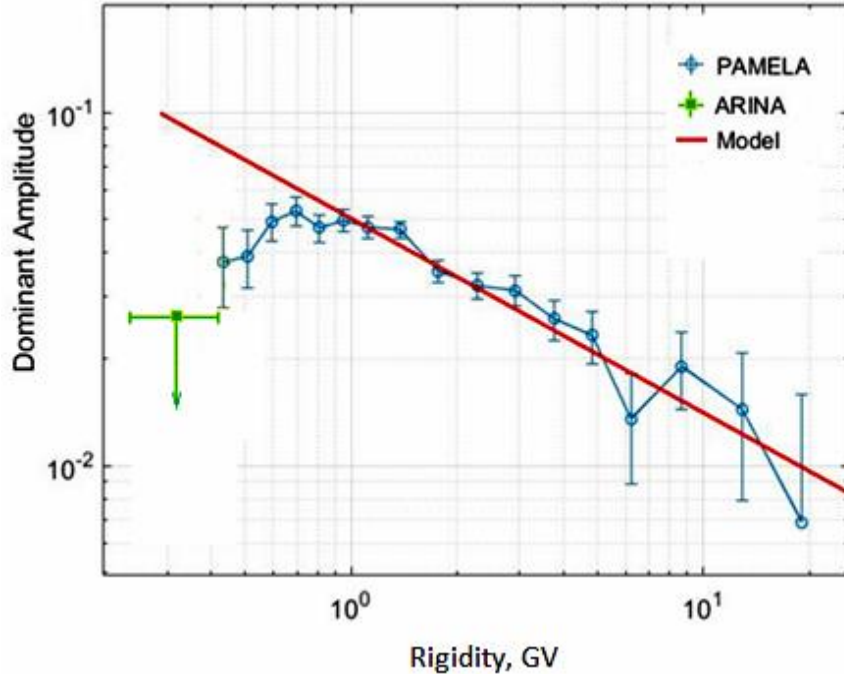


Fig. 1. Dependence of the maximum amplitude of 27-day variations of the galactic proton flux on the rigidity of particles.

This result about 27-day GCRs variations lead us to the conclusion that the transport of galactic particles is significantly different for low and high energies and depends on the modulation region characteristics in the interplanetary space. We looking for further investigation of this interesting problematic.